

RESEARCH

Open Access



Investigation of nanotopography on SOCE mediated cell migration via live-cell Imaging on opaque implant surface

Yan Zhang^{1†}, Kai Li^{2†}, Guangwen Li^{1†}, Yazheng Wang³, Yide He^{4*}, Wen Song^{1*} and Yumei Zhang^{1*}

Abstract

The exploration of cell response to nanotopography has attracted considerable attentions for years. This article focuses on the influence of nanotopography on the intracellular Ca^{2+} dynamics, the most ubiquitous but ignored second messenger. The classic titanium nanotubes (NT) were fabricated by anodization to formulate nanoporous surfaces. Firstly, the store operative calcium entry (SOCE) in endoplasmic reticulum (ER) and functional Ca^{2+} release-activated Ca^{2+} (CRAC) channels were significantly enhanced on NT surfaces that revealed by live-cell Ca^{2+} imaging and fluorescence resonance energy transfer (FRET) identification of orai1-stim1 connection. To investigate the potential implication of Ca^{2+} elevation, the dynamic cell migration trajectory was monitored by a self-made holder, which could not only be suitable for the opaque implant surface but also guarantee the focus fields identical during samples shifting. The cell migration on NT surface was more vigorous and rapid, which was correlated with higher focal adhesion proteins expression, Ca^{2+} -dependent calpain activity and stim1 level. In conclusion, this study has confirmed the novel ER Ca^{2+} hemostasis pathway on nanosurfaces and its crucial role in cell migration regulation, which may help for more biofavorable implant surface design.

Keywords Nanotopography, SOCE, Cell migration, Live-cell imaging, Opaque surface, Stim1

Introduction

The cell response to nanotopography has attracted considerable attentions for years [1, 2]. It is not only a bridge between nanotechnology and biological behaviors, but also contribute to the biomedical devices surface design.

In the orthopedic implant area, the implant surface nanotopography is known to be prominent for guiding various cell types that contributing to the final osseointegration [3, 4]. For instance, the bone mesenchymal stem cells (BMSCs) are prone to osteogenic differentiation in contact with mild chaotic nanotopography [5]. The macrophages polarization is also directed by nanotopography and contributing to osteogenesis through cytokines secretion, which is also known as the osteoimmunology [6]. In the meanwhile, the mechanism of how the extracellular physical pattern signaling is transferred into cells is also fascinating. Generally, there are several different directions for the explanations. A common direction is mechanical force driven cell deformation. The different nanotopographies may be sensed as different

[†]Yan Zhang, Kai Li and Guangwen Li contributed equally to this work.

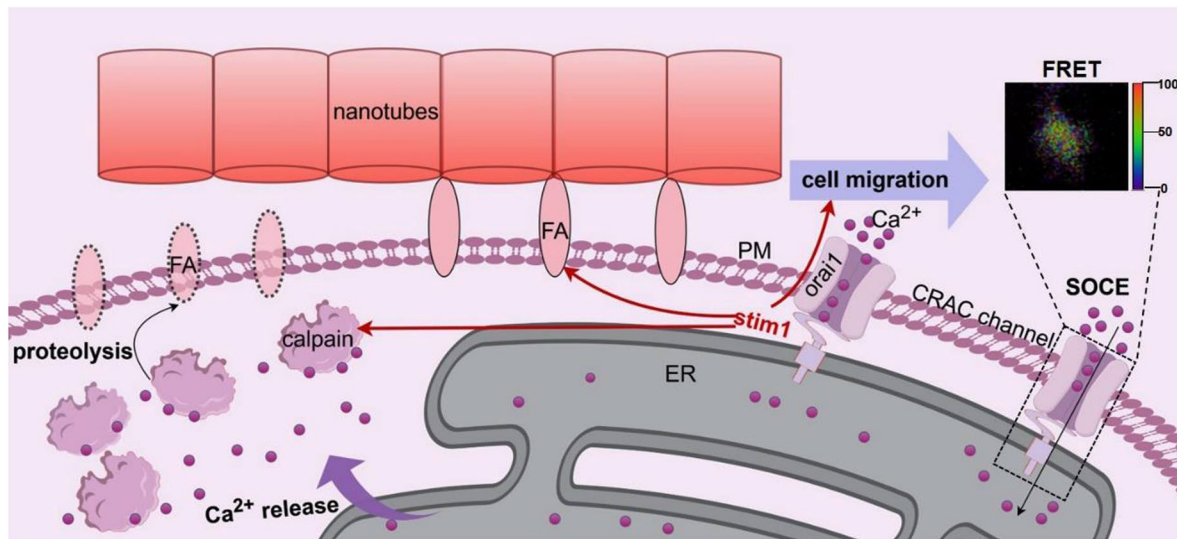
*Correspondence:

Yide He
heyide1227@126.com
Wen Song
wensong71@163.com
Yumei Zhang
wqtzym@fmmu.edu.cn

Full list of author information is available at the end of the article



© The Author(s) 2023, corrected publication 2023. **Open Access** This article is licensed under a Creative Commons Attribution 4.0 International License, which permits use, sharing, adaptation, distribution and reproduction in any medium or format, as long as you give appropriate credit to the original author(s) and the source, provide a link to the Creative Commons licence, and indicate if changes were made. The images or other third party material in this article are included in the article's Creative Commons licence, unless indicated otherwise in a credit line to the material. If material is not included in the article's Creative Commons licence and your intended use is not permitted by statutory regulation or exceeds the permitted use, you will need to obtain permission directly from the copyright holder. To view a copy of this licence, visit <http://creativecommons.org/licenses/by/4.0/>. The Creative Commons Public Domain Dedication waiver (<http://creativecommons.org/publicdomain/zero/1.0/>) applies to the data made available in this article, unless otherwise stated in a credit line to the data.

Graphical Abstract

mechanical force that resulting in the alterations of membrane rigidity [7], cytoskeleton arrangement [8, 9] and nucleus deformation [10]. For example, nanoscale surface topography reduces cell stiffness by enhancing integrin endocytosis [7]; Silicon nanoneedle affects nuclear envelope integrity [10]. The responses of cells are critically influenced by different diameters or dimensions of the nanostructure, which is also the outcome of mechanical force driven cell deformation. Adhesion, proliferation, migration, and differentiation of mesenchymal stem cells (MSCs) are maximally induced on 15-nm nanotubes, but prevented on 100-nm nanotubes, which induces cell death [11]. The hydrophilicity is also involved, which contributes to the clinical success of dental implant [12–14]. For instance, cells on hydrophilic modified sand-blasted acid etched titanium surfaces display enhanced adhesion and spreading, as well as increased proliferation [12]. A hydrophobic characteristic has been shown to be a more general characteristic of microstructured titanium [15, 16], while the existence of nanostructures was proven on hydrophilic blasted/etched implant surfaces [15]. Some studies focus on conventional molecular biological regulations feedback, such as Wnt signaling [17], and Mitogen-activated protein kinase (MAPK) pathway [18]. Certain extracellular proteins adsorption on different nanopographies may act as different signaling transduction cascade to initiate the downstream molecular reactions. Previously, our group has also revealed the mechanotransduction pathway mainly from this direction in various cell types [19–21].

Compared to biomolecules, ions are more extensively distributed in vivo. However, the ions mediated cell behavior has not arisen sufficient concentration. As a second messenger, calcium ions (Ca^{2+}) impact nearly all aspects of cellular physiology [22]. Various different Ca^{2+} channels finely maintain and control the Ca^{2+} concentrations at different places to regulate specific cellular activities. Our previous study has confirmed the store operated Ca^{2+} entry (SOCE) in endoplasmic reticulum (ER) has crucial role for osteogenic differentiation control by titania nanotubes array [23]. Depletion of ER Ca^{2+} into cytosol through inositol 1,4,5-trisphosphate receptor (IP3R) is the most efficient way to increase cytosolic Ca^{2+} level for triggering the following Ca^{2+} dependent molecules interaction [24]. Apart from cell differentiation, the SOCE process is mostly validated for cell migration regulation [25, 26], which is a prerequisite step post cell adhesion on biomaterial surface. In the meanwhile, the ions oscillations are often transient at minutes scale and dependent on living status. Limited by normal imaging techniques, it is difficult to monitor ions alterations in living cells on untransparent biomaterial surface, such as the metallic implant surface.

In the present study, we have fabricated two devices for living cells imaging on untransparent biomaterial surface by confocal microscopy. The cytosolic Ca^{2+} oscillations and SOCE process were successfully captured on titanium implant surface with different nanopographies. Meanwhile, their relevance to cell migration was also monitored through live cell trajectory mapping. This

work not only for the first time directly revealed the Ca^{2+} alterations and endoplasmic reticulum and plasma membrane (ER-PM) contact site that interpreted by nanotopography, but also implied a new unfiled but important area for the investigation of cell responses to biomaterial surface.

Experimental section

Titanium (Ti) samples Preparation and characterization

Pure Ti plates (99.997% purity, diameter=15 mm, thickness=1 mm) were provided by Baoji Nonferrous Metals Industry Corporation (Baoji, China). Then, the samples were polished from 400 to 7000 meshes with SiC sandpaper and ultrasonically cleaned sequentially in acetone, absolute ethanol, and deionized water to produce the polished Ti (PT) surface. The nanotube topography (NT) was obtained on PT surface via anodization in 0.5 wt% hydrofluoric acid at either 5 V (NT5) or 20 V (NT20) for 1 h [6, 27]. The field-emission scanning electron microscope (FE-SEM; Hitachi Ltd, Japan) was used to observe the surface morphology. All samples were sterilized with 75% ethanol prior to cell culture.

Cell culture

The primary murine bone marrow mesenchymal stem cells (mBMSCs) were used in this study and all the animal experimental protocols were approved by the Animal Ethics Committees of the Fourth Military Medical University. Briefly, the femurs and tibias of male C57BL/6 mice aged 6–8 weeks were isolated. The bone marrow contents were flushed out from the diaphysis with Minimum Essential Medium Alpha basic (α -MEM, Gibco, USA) supplemented with 20% fetal bovine serum (FBS, InCellGenE, USA), and 1% penicillin-streptomycin (HyClone, USA), and filtered by cell strainer of 100 μm . After 4 days culture, half of the medium was refreshed, and after 6 days, all the medium was refreshed. When the cells reached to ~80% confluence, the mBMSCs were trypsinized using 0.25% trypsin (Gibco) for passage culture. The passage 2 and 3 of cells were used in the experiments.

Cytosolic Ca^{2+} measurement

For Ca^{2+} imaging, cells on Ti samples were incubated with 10 μM FLUO-8 AM (Abcam, UK) for 30 min. Then the cells were imaged by confocal laser scanning microscope (Olympus, Japan) in Ca^{2+} -free medium containing 140 mM NaCl, 5 mM KCl, 1 mM MgCl_2 , 10 mM glucose (all from the Sinopharm Chemical Reagent Co., Ltd, China), 10 mM HEPES, and 20 μM EGTA (both from Sigma, USA), with or without Ca^{2+} release-activated Ca^{2+} (CRAC) inhibitor CM4620 (10 μM , MCE, USA). An ultra-thin Ti cross (side length 19 mm, thickness

0.45 mm) was used to support the samples in order to allow fluids exchange in the gap between glass bottom and living cells. The observation time-frame was 10 min for each sample, consisting of 1 min adaption, 4 min Thapsigargin (TG, 2.5 μM , Invitrogen, USA) treatment, and 5 min Ca^{2+} (2 mM, Sinopharm Chemical Reagent Co., Ltd) recovery.

Transmission electron microscopy (TEM) examination

After cultured for 24 h, 7×10^6 cells on the surface of each group were collected using 0.25% trypsin (Sigma) and fixed in 2.5% glutaraldehyde, postfixed with 1% osmium tetroxide, dehydrated in ethanol, and embedded in Epoxy. After sectioning, the intracellular ER and plasma membrane (PM) structure were observed in a transmission electron microscope (FEI, USA).

Fluorescence resonance energy transfer (FRET) measurement

FRET was performed on confocal laser scanning microscope (Nikon Instruments Inc., USA). For GFP and mCherry excitation, 445 and 514 nm lasers were chosen respectively. GFP and mCherry fluorescent signals were collected at 465–505 nm and 518–558 nm separately. Throughout the data acquisition process, samples were maintained at room temperature.

For FRET measurement, mBMSCs were infected by lentiviruses of only orai1-GFP, only stim1-mCherry, and both orai1-GFP and stim1-mCherry respectively. After 3 days, the cells were collected using 0.25% trypsin (Sigma) and seeded on different surfaces. After 24 h, the samples were inverted on the titanium cross in the confocal dishes containing Ca^{2+} -free medium. The observation time-frame was 9 min for each sample, consisting of 1 min adaption, 4 min TG (2.5 μM , Invitrogen) treatment, and 4 min Ca^{2+} (2 mM, Sinopharm Chemical Reagent Co., Ltd) recovery. Time-lapse images were captured every 30s for a 9 min period. The final datasets were analyzed using the FRET module in the Nikon NIS-Elements software, and calibrated according a previously published method [28]. At last, the average FRET efficiency was obtained from the FRET module and used for statistical analysis.

Cell trajectory tracking

The cells were seeded on different surfaces for 24 h. Next, the cell plasma membrane was stained by Cell Plasma Membrane Staining Kit with DIO (Green fluorescence) (Beyotime, China) according to the instructions. Then the specimens were mounted in a novel self-made holder, which was precisely suitable for 24-Well Glass Bottom Black Plate with Lid (Cellvis, USA). The cells were cultivated in a live-cell incubation chamber

mounted on a live-cell workstation (Tokai Hit, Japan). The temperature and atmosphere conditions inside the chamber were controlled to be the same as the cell incubator. Live-cell time-lapse imaging was performed on confocal laser scanning microscope (Nikon Instruments Inc.). Cell images were captured every 15 min for a total duration of 12 h. To quantify cell migration, cell images were imported into the ImageJ software, and the manual tracking function in ImageJ software was used to obtain the trajectory of cell, including the coordinates and length of the trajectory. Then, the position plots of the cell sites were mapped to a common origin using MATLAB software.

Immunofluorescence staining

The visualization of the desired focal adhesion (FA) proteins including Vinculin and FAK was carried out by immunofluorescent staining. The cells were seeded on different surfaces at the density of 1×10^5 cells per sample and cultured for 24 h. Then the cells were gently rinsed with phosphate-buffered saline (PBS; HyClone, USA) and fixed with 4% paraformaldehyde. After permeabilized with 0.1% Triton X-100 for 10 min, the cells were blocked with 5% goat serum albumin (Boster, USA) for 30 min. Then the cells were incubated with anti-vinculin antibody (1:100, Abcam) or anti-FAK antibody (1:400, Proteintech, USA) at 4 °C overnight. The cells were labeled with Dylight 488, goat anti-rabbit IgG second antibody (1: 200, Abbkine, USA) for 2 h at 37 °C. Finally, the cells were mounted by Antifade Mounting Medium with DAPI (Beyotime) and imaged using confocal laser scanning microscope (Nikon Instruments Inc.). The fluorescent intensity of the cells was analyzed using the ImageJ software.

Calpain activity

The cells were seeded on different surfaces at the density of 2×10^5 cells per sample and cultured for 24 h. After rinsed with PBS, the cells were incubated with 10 μ M CMAC peptidase substrate, t-BOC-Leu-Met (Invitrogen) at 37 °C for 30 min. The blue fluorescence of t-BOC-Leu-Met cleavage products by calpain was dynamically examined in living cells under Ca^{2+} -free condition by confocal at Ex/Em of $\sim 351/430$ nm.

Statistical analysis

All data were expressed as mean \pm SD, and at least three independent experiments for each group were performed. The statistical analysis was conducted using GraphPad Prism 8.0 software. The results were analyzed by one-way ANOVA and Tukey's post hoc tests. A p value less than 0.05 is statistically significant.

Results and discussion

CRAC channels participate in SOCE on Ti surfaces and SOCE level is up-regulated by NT

Uniform TiO_2 tubular nanostructure could be observed on both the surfaces of NT5 and NT20, and the inner diameters of the nanotubes were about 25 and 80 nm respectively (Fig. 1A). The NT surface also showed hydrophilic property with increased roughness (Fig. S1), which was in line with our previous sample surfaces. In order to realize in situ observation of living cells on opaque Ti surfaces, a specially designed Ti cross was applied. The Ti cross with 0.45 mm thickness was used to support the inverted Ti plate seeded with cells, which could ensure the cells to be in the confocal focusing range without any pressure and the quick spreading of the drug added to the confocal dish (Figs. 1B and S3). To verify if TG induced Ca^{2+} influx on Ti surfaces was through CRAC channels, a CRAC channel inhibitor, CM-4620 was applied. CM-4620 showed inhibition effects on Ca^{2+} influx both in ER Ca^{2+} depletion stage induced by TG and Ca^{2+} recovery stage in all the three surfaces (Fig. 1C and D). Next, the impact of NT on cytosolic Ca^{2+} level was investigated. Ca^{2+} level was significantly higher in NT5 and NT20 compared with PT, and NT5 showed the highest Ca^{2+} level (Fig. 1E and F).

The rise in cytosolic Ca^{2+} level caused by NT may come from two ways, entry across the plasma membrane or release from intracellular stores [29]. The cells on nanotubes are forced to elongate and stretch to search for protein aggregates, thus exposed to more stress and changes in membrane tension compared to PT [30]. So the mechanosensitive ion channels may altered in response to changes in membrane tension and curvature [31], leading to elevated intracellular calcium levels [32]. ER is recognized as an important intracellular Ca^{2+} store [33]. Meanwhile, IP_3R -mediated ER Ca^{2+} release participates in overall intracellular Ca^{2+} signaling network and regulates fundamental cellular function [24]. SOCE, activated by reduction of free $[\text{Ca}^{2+}]_{\text{ER}}$, has been reported to play an important role in many physiological activities, such as spatiotemporal control of gene expression, maintenance of immune function, and cell migration [34]. So, the above experimental results indicates that the ER Ca^{2+} release may play critical physiological role, which implies the importance of further analyzing SOCE in ER.

As the constituent molecules of CRAC channels, orai proteins are identified as store-operated Ca^{2+} channels and stim proteins are identified as Ca^{2+} sensors for SOCE [34]. There are three homologues for orai, the orai1/2/3, and two homologues for stim, the stim1/2. Although

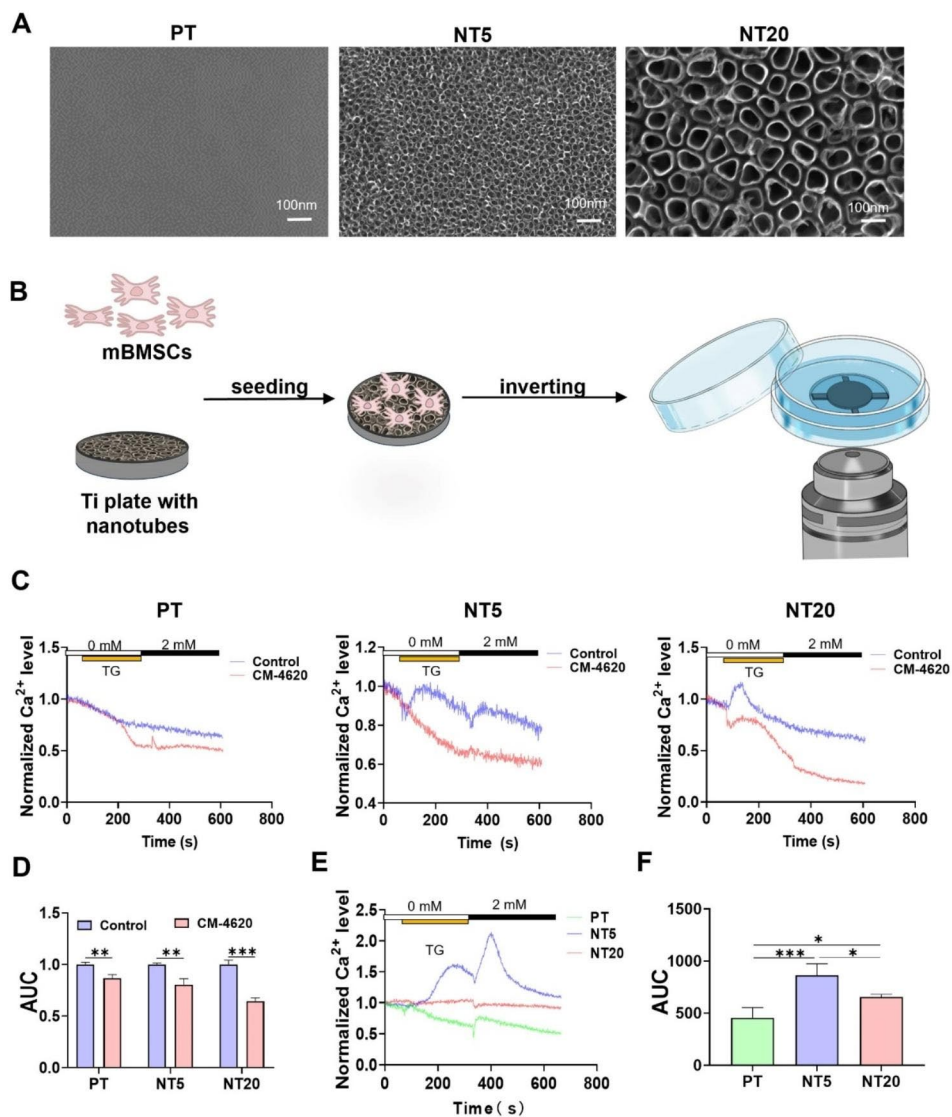


Fig. 1 Observation the SOCE on different Ti surfaces via Ti cross which was used to assist in observing living cells on the surface of opaque materials. **(A)** FE-SEM images of the sample surfaces. **(B)** Schematic diagram of observing calcium ion oscillation in living cells on the surface of titanium samples using laser confocal microscope and assisted by Ti cross. **(C)** Calcium traces of the cells on Ti plate treated with CM-4620, when the fluorescence of Calcium was monitored, the 2.5 μ M TG was added, following by 2mM Calcium. **(D)** The quantification of the area under the curve (AUC) ($n=3$). **(E, F)** Calcium fluxes and AUC following stimulation with TG and 2 mM calcium in mBMSCs on different surfaces ($n=4$). Data are presented as mean \pm SEM, Student's t-test or One-way ANOVA, * $P \leq 0.05$, ** $P \leq 0.01$, *** $P \leq 0.001$

orai1 and stim1 are reported to be the key components of CRAC channel [35], orai2/3 and stim2 also contribute to SOCE through different ways [36, 37]. Therefore, which subtypes dominated on NT surface should be confirmed.

Polymerase chain reaction (PCR) examination of the dynamic mRNA levels, orai1 and Stim1 were most sensitive to time compared with orai2/3 and stim2 in NT5 and NT20, while there were no significant differences in the expression of orai1/2/3 and the expression of stim1/2 at different times in PT (Fig. S4A and B).

Thus, orai1 and stim1 were selected as the target proteins for following observation. Compared with 3 and 7 days, at 1 day, the difference of orai1 or stim1 among PT, NT5 and NT20 was the greatest (Fig. S4C). Therefore, 1 day was selected as the target time point for subsequent observation. Meanwhile, NT had promoted the expression of orai1 and stim1 compared with PT, and the expression of stim1 in NT5 was higher than that in NT20 (Fig. S4C), this could also partially explain the elevated cytosolic Ca^{2+} in NT5 and NT20, especially the NT5.

NT enhances FRET efficiency between Orai1 and Stim1

Orai1 is expressed in plasma membrane and stim1 is expressed in the ER membrane. After depletion of ER Ca^{2+} , the stim1 and orai1 redistribute within their respective membrane and coaccumulate in clusters to activate SOCE [38]. The sites of coaccumulation are ER-PM junctions, where ER is held close enough but not fused to the PM, and the average ER-PM gap is reported to range from 10 to 17 nm [39]. So the observation of ER-PM

junctions can partially reflect the relative positional relation between orai1 and stim1. ERs were observed to be more swollen in NT5 and NT20 than PT, and NT5 was more pronounced than NT20 (Fig. 2A). And this result is agreed with our previous research that ER could suffer from different stress states triggered by morphological factors [23, 40]. Then ER stress leads to Ca^{2+} releasing from ER to cytosol [41], which is also responsible for the high Ca^{2+} cytosolic level in NTs, especially the NT5.

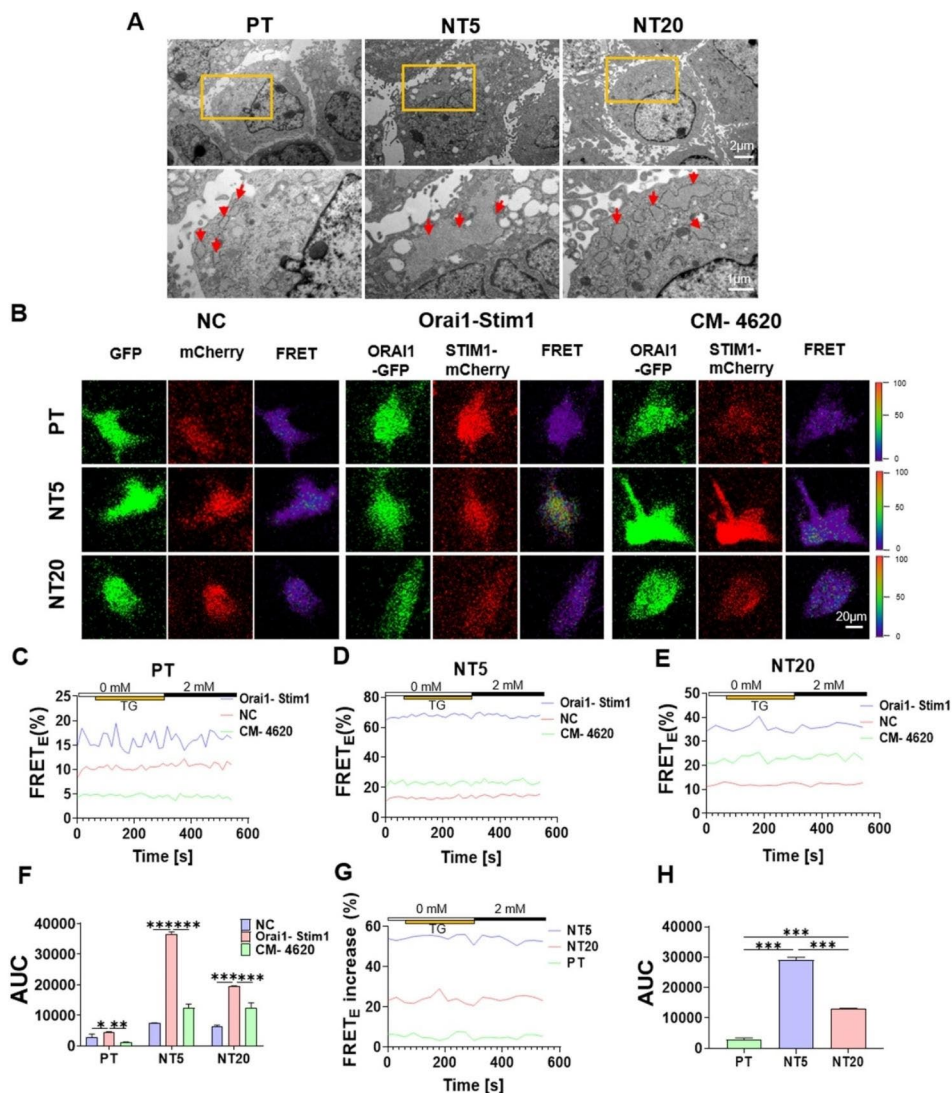


Fig. 2 Influence of Ti nanotopographies on the endoplasmic reticulum and FRET between Orai1 and Stim1 in mBMSCs. **(A)** ER and PM observation in mBMSCs on different surfaces by TEM. **(B)** Presentative images of FRET efficiency between orai1-GFP and stim1-mCherry with or without CM-4620 on surfaces of PT, NT5, NT20 at 0 s. **(C-E)** FRET efficiency analysis of the time course of interactions between orai1-GFP and stim1-mCherry with or without CM-4620 on surfaces of PT, NT5, NT20, when the fluorescence was monitored, the 2.5 μM TG was added at 60 s, following by 2mM Calcium at 300s, **(F)** and the quantification of the area under the curve (AUC). **(G)** FRET efficiency increase of the time course of orai1-stim1 group compared with NC group between different surfaces **(H)** and the quantification of the AUC. Data are presented as mean ± SEM, n = 3, Student's t-test or One-way ANOVA, ns, not significant, *P ≤ 0.05, **P ≤ 0.01, ***P ≤ 0.001

However, no typical ER-PM junctions were observed in both NT5, NT20 and PT using TEM (Fig. 2A), which may be due to the digestion procedure. Thus, the in-situ FRET observation was performed.

As a highly effective means of studying protein interactions [42], FRET was used to explore the positional relation between *orai1* and *stim1* based on in situ live-cell observation. FRET occurs in a short range (5-10 nm) across which energy is transferred from an excited donor to acceptor fluorophore [42]. Firstly, FRET phenomenon was verified emerging in both PT, NT5 and NT20, and occurring between *orai1* and *stim1* by adding CRAC inhibitor, the CM4620 (Fig. 2B-F). NT could promote the FRET efficiency between *orai1* and *stim1* compared with PT, especially the NT5 (Fig. 2B, G, H). Comparing with PT, the stronger expression of *stim1* in NT5 and NT20 (Fig. S4C), especially in NT5, can partially explain the higher FRET efficiency in NT5 and NT20, especially in NT5. However, with the addition of TG and Ca^{2+} , no evident fluctuation of FRET efficiency was occurred (Fig. 2G).

It is speculated that in order to maintain the basic functions of cells, Ca^{2+} is occasionally discharged from ER into cytoplasm, and the Ca^{2+} restoration in ER is replenished through CRACs. Nevertheless, due to the Ca^{2+} free medium used in this experiment, no Ca^{2+} could be replenished to ER. So it is speculated that the low ER Ca^{2+} will activate all functional CRAC channels, which resulting in no increase in FRET efficiency even after TG addition. Even the addition of Ca^{2+} can't induce any change in FRET efficiency, as SOCE may be not ending in 5 min [34], thus the CRAC channels are keeping activated.

Cell Migration speed and length are promoted by NT surface through Stim1

Previous studies have confirmed the alterations of ER SOCE and specific *orai1-stim1* approaching pattern induced by NT surface, it is reasonable to elucidate their biological implications. Accordingly, Ca^{2+} signaling is vastly related to cell adhesion and migration, in which *stim1* expression is directly associated with tumor cells invasiveness and embedding [43]. In the meanwhile, the cell migration is also a prerequisite process post cell contact with implant surface. Therefore, the role of *stim1* in the cell migration regulation on NT surface was investigated.

Collective cell migration experiments were tried firstly to explore the motility of mBMSCs. The mobility of mBMSCs on NT5 and NT20 surfaces was obviously

increased compared to PT surface (Fig. S6). In order to realize in situ observation of living cells migration on opaque materials, a specially designed holder was applied (Figs. 3A and S8). The holder could keep the Ti samples stable during the rapid movement of plate, which guaranteed the multiple focused areas unchanged. mBMSCs exhibited the most vigorous motility on NT5 surface, followed by NT20, and the last was PT, as displayed in the trajectory analysis obtained from the time-lapse imaging (Figs. 3B and S9A). In addition, the cell migration was increased or decreased after *stim1* overexpression or inhibition, except for NT5 that the migration was not increased anymore after *stim1* overexpression (Figs. 3C, S9B, C).

It is consistent with previous reports that NT promoted cell migration [44–46]. It has been verified that cell migration is induced by dynamically regulated of the assembly and disassembly of FA proteins [47]. Meanwhile calcium influx has been linked to FA turnover during cell migration [48]. Therefore, it can be speculated that different calcium levels in NT20, NT5 and PT may lead to different FA dynamics, resulting in different migration behaviors mentioned above. However, there is a limit for the influence of Ca^{2+} , so the cell migration in NT5 doesn't continue to increase after overexpression of *stim1*.

Focal Adhesion Proteins are upregulated on NT surface and regulated by Stim1

The focal adhesion proteins of vinculin and FAK were observed by immunofluorescent staining. Comparing with PT, the expressions of vinculin and FAK were promoted by NT5 and NT20, with NT5 having the strongest expression (Fig. 4A-D). They were also upregulated after *stim1* overexpression, except for NT5 (Fig. 4E, F, I, J). Meanwhile, the expressions of vinculin and FAK in all three groups were inhibited after *stim1* knock-down (Fig. 4G, H, K, L).

For poorer hydrophilicity was exhibited in PT than NT5 and NT20 (Fig. S1A), there may be lower population of serum proteins aggregating on the surface of PT [30], which is adverse to the formation of FA. The stronger expression of FAs in NT5 compared to NT20 may be explained by two reasons. On the one hand, the protein aggregates initially attach only to the available surfaces that are the top portion of the nanotube walls [30], and the adhesion of proteins (≈ 30 -nm-size regime) initially determines the degree of cell adhesion. The nanopores with a diameter of 25 nm (NT5)

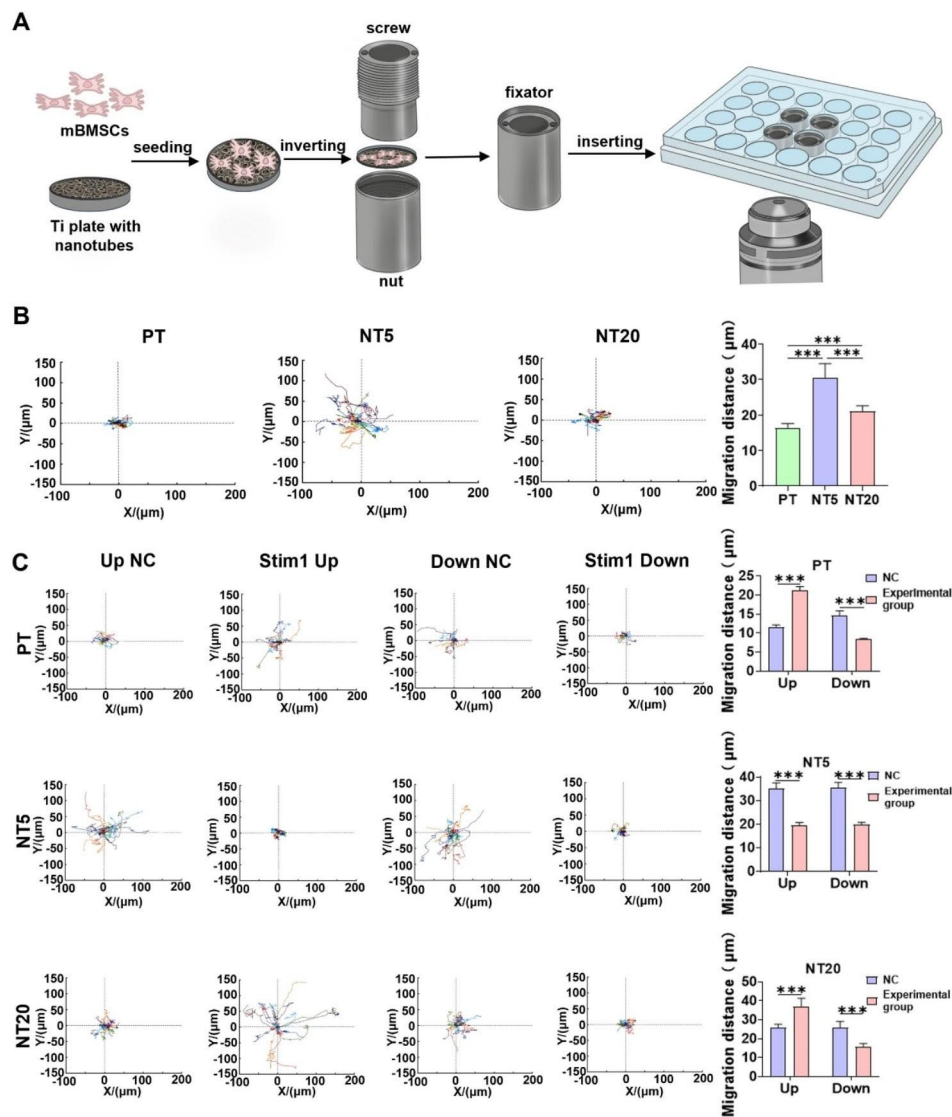


Fig. 3 Influence of Ti nanotopographies and stim1 on the migration of single cell. **(A)** Schematic diagram of observing single cell migration on the surface of titanium samples using laser confocal microscope and assisted by self-made holder. **(B)** The single cell migration trajectory on different surfaces, and position plots of the cell sites mapped to a common origin, which showed fifteen typical cells in each group. Each site represents the time-dependent position of the center of the nucleus of a single cell. And the quantification of the cell migration distance on different surfaces ($n = 22$). **(C)** The single cell migration trajectory after knockdown or overexpression of stim1 on three surfaces and the quantification of the cell migration distance ($n = 15$). Data are presented as mean \pm SEM, Student's t-test or One-way ANOVA, ns, not significant, * $P \leq 0.05$, ** $P \leq 0.01$, *** $P \leq 0.001$

are suitable for ≈ 30 -nm size serum protein aggregates to anchor on, while the nanopores with a diameter of 80 nm (NT20) are too large for the serum proteins to aggregate to anchor on. On the other hand, since lateral spacing of integrin ligands influencing FA assembly [49], and the lateral spacing of integrin ligands less than 50–70 is essential for the assembly of FA and stress fibers [50], therefore 80-nm diameter nanopores

(NT20) will inhibit the assembly of FA compared to 25-nm diameter nanopores (NT5). It is showed in studies that the ER protein colocalizes with adhesion sites, and the transportation of ER tubules along microtubules to contact FAs is indeed crucial to support FA growth [51, 52]. Therefore, it is speculated that there were more colocalizations of ER protein with FA, which means more ER distributing near the

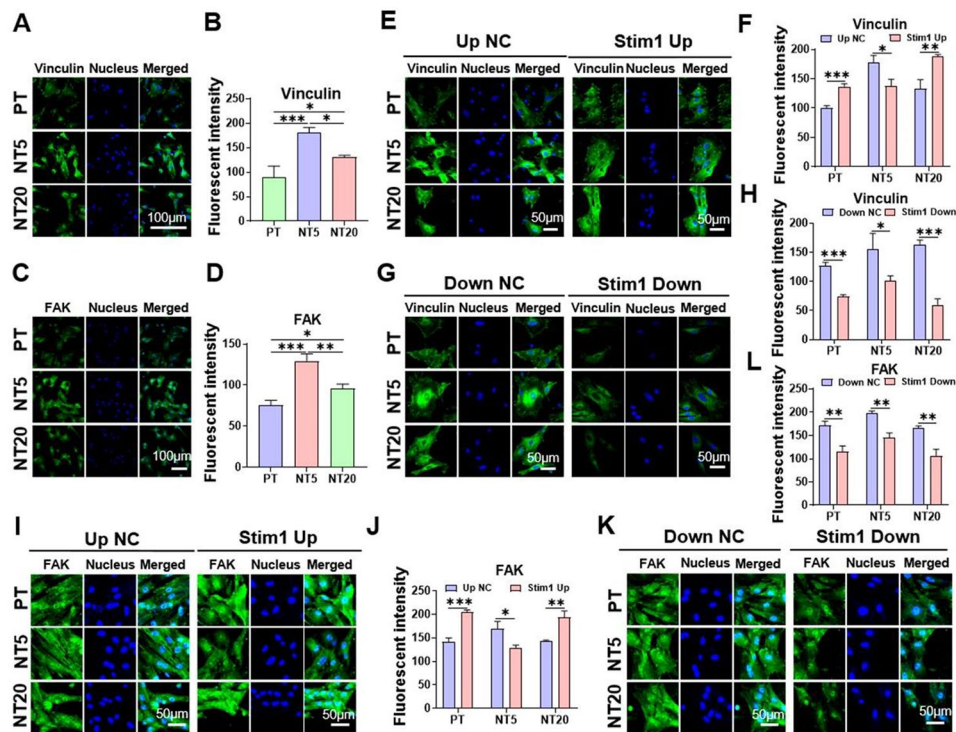


Fig. 4 Influence of Ti nanotopographies and stim1 on FAK and Vinculin of mbMSCs. (A) Immunofluorescence staining depicts the expression of vinculin on different surfaces (B) and the quantification of fluorescence intensity of vinculin. (C) Immunofluorescence staining depicts the expression of FAK on different surfaces (D) and the quantification of fluorescence intensity of FAK. (E–H) The expression of vinculin on different surfaces after overexpression (E) or knockdown (G) of stim1 exhibited by immunofluorescence staining, and the quantification of fluorescence intensity of vinculin (F,H). (I–L) The expression of FAK on different surfaces after overexpression (I) or knockdown (K) of stim1 exhibited by immunofluorescence staining, and the quantification of fluorescence intensity of vinculin (J,L). Data are presented as mean \pm SEM, $n = 3$, Student's *t*-test or One-way ANOVA, * $P \leq 0.05$, ** $P \leq 0.01$, *** $P \leq 0.001$

plasma membrane. This may be responsible for the highest FRET efficiency between *orai1* and *stim1* in NT5.

Since the calpain family of protease has been reported to regulate cell motility by degrading FA and promoting rear detachment [53], the NT may affect the activity of calpain. If the assumption comes into existence, similarly, is effect of NT on cell migration ultimately achieved through the regulation of calpain activity by *stim1*?

Calpain activity is increased on NT surface and regulated by Stim1

The *t*-BOC-Leu-Met was used to measure the calpain activity in live-cells on different surfaces of Ti samples, with the assistance of Ti cross mentioned above. It was

found that NT5 and NT20, especially NT5 can largely promote the activity of calpain compared to PT (Fig. 5A–C). The overexpressed *stim1* could promote the activity of calpain in all three groups (Fig. 5D–H). The activity of calpain was decreased by knocking down *stim1* in all three groups (Fig. 5I–M).

As calpain exhibits calcium-dependent protease activity, the high level of calcium in NT5 and NT20, especially NT5, can explain the promotion of NT5 and NT20, especially NT5, on the activity of calpain. For overexpressed *stim1* may improve SOCE [26], this may explain the high activity of calpain in all three groups. But the hyperactivity of calpain after *stim1* being overexpressed in NT5 may result weak FAs in NT5, which is likely to lead to less stable protrusions, thus explains the decrease motility of cells in NT5 [54].

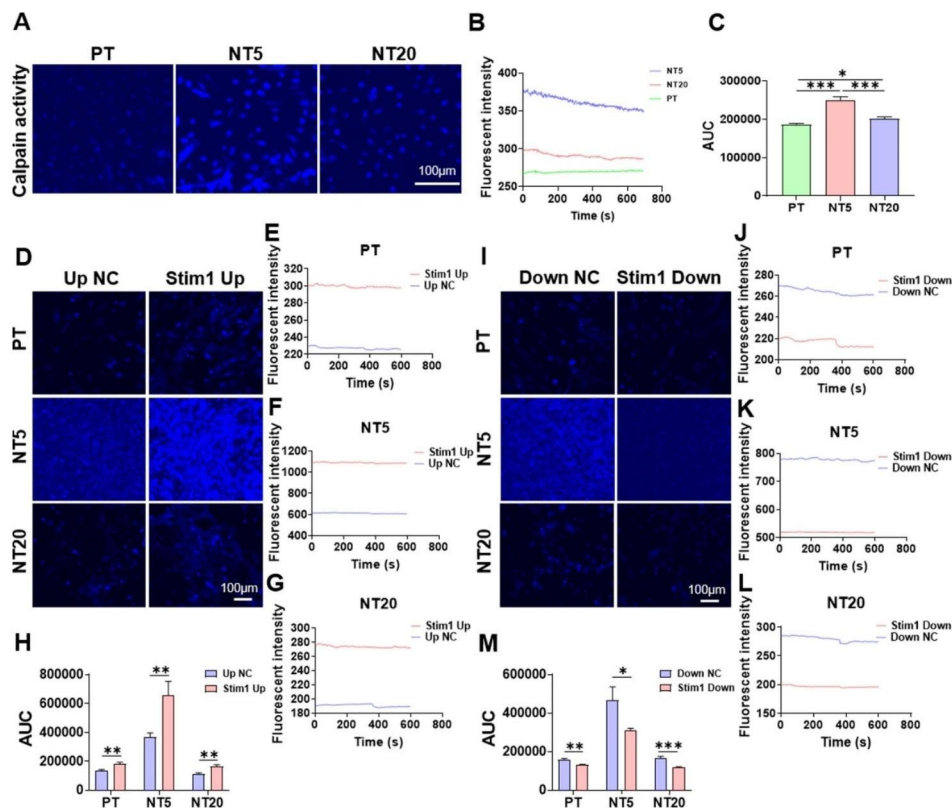


Fig. 5 Influence of Ti nanotopographies and stim1 on the activity of calpain of mBMSCs. (A) mBMSCs on different surfaces were treated with t-BOC-Leu-Met, which is an artificial fluorogenic calpain substrate, for 30 min. And each sample were observed for 10 min, the confocal images at 0 s were exhibited. (B) The time course of fluorescent intensity which represents the time course of calpain activity of mBMSCs on different surfaces. (C) and the quantification of the area under the curve (AUC). (D) mBMSCs overexpressing stim1 on different surfaces were treated with t-BOC-Leu-Met, and each sample were observed for 10 min, the confocal images at 0 s were exhibited. (E-G) The time course of fluorescent intensity of mBMSCs overexpressing stim1 on different surfaces, (H) and the quantification of the AUC. (I) mBMSCs with stim1 knockdown on different surfaces were treated with t-BOC-Leu-Met, and each sample were observed for 10 min, the confocal images at 0 s were exhibited. (J-L) The time course of fluorescent intensity of mBMSCs with stim1 knockdown on different surfaces, (M) and the quantification of the area under the curve (AUC). Data are presented as mean \pm SEM, Student's t-test or One-way ANOVA, * $P \leq 0.05$, ** $P \leq 0.01$, *** $P \leq 0.001$

Conclusion

The study lively revealed the Ca^{2+} oscillation driven by ER SOCE process on opaque implant surface, and its significance on cell migration regulation. In brief, the ER SOCE process was enhanced on nanoporous surface, which accounted for the vigorous cell migration through stim1 upregulation. The findings may not only help to better understand the Ca^{2+} homeostasis induced by nanotopographies, but also imply a method for acquiring concrete living cell information on opaque biomaterial surface. As a classic titanium nanomaterial, NT5 with a diameter of 25nm can better promote early migration of mBMSCs than NT20 with a diameter of 80nm. This may provide a theoretical basis for promoting early osseointegration of implant, but further validation is needed through in vitro and in vivo experiments.

Abbreviations

NT	titanium nanotubes
SOCE	store operative calcium entry
ER	endoplasmic reticulum
CRAC	Ca^{2+} release-activated Ca^{2+}
FRET	fluorescence resonance energy transfer
BMSCs	bone mesenchymal stem cells
MSCs	mesenchymal stem cells
MAPK	Mitogen-activated protein kinase
Ca^{2+}	calcium ions
IP3R	inositol 1,4,5-trisphosphate receptor
ER-PM	endoplasmic reticulum and plasma membrane
PT	polished Ti
NT	nanotube topography
NT5	anodization in 0.5 wt% hydrofluoric acid at 5 V
NT20	anodization in 0.5 wt% hydrofluoric acid at 20 V
FE-SEM	field-emission scanning electron microscope
mBMSCs	murine bone marrow mesenchymal stem cells
α -MEM	Minimum Essential Medium Alpha basic
FBS	fetal bovine serum
TG	Thapsigargin
PM	plasma membrane
FA	focal adhesion
PBS	phosphate-buffered saline
PCR	Polymerase chain reaction
AUC	area under the curve

Supplementary information

The online version contains supplementary material available at <https://doi.org/10.1186/s12951-023-02249-8>.

Supplementary Material 1: Fig. S1. Characterizations of the Ti samples. ** $P \leq 0.01$, *** $P \leq 0.001$. **Fig. S2.** Identification of the multidirectional differentiation potential of MBMSCs, osteogenic differentiation and adipogenic differentiation. **Fig. S3.** The diagram and physical images of the titanium cross used to assist in confocal imaging of live-cells. **Fig. S4.** Screening of subtypes of constituent Molecules of functional store-operated CRAC channels that are most sensitive to time on Ti surfaces, and screening of the most sensitive time points for changes in these subtypes. * $P \leq 0.05$, ** $P \leq 0.01$, *** $P \leq 0.001$. **Fig. S5.** Determination of the optimal multiplicity of infection (MOI) for lentivirus transfection, Ori1-GFP, Stim1-mCherry. **Fig. S6.** Influence of Ti nanopatterns on collective cell migration at 0 h, 6 h, 12 h, 24 h, 48 h. Green-F-actin; Blue-nuclei. **Fig. S7.** Screening of stim1 knockdown within three guarantees and validation of RNA levels after stim1 knockdown and overexpression. *** $P \leq 0.001$. **Fig. S8.** The diagram and the physical image of the holder used to assist in confocal imaging of live-cells. **Fig. S9.** The live-cell time-lapse imaging and single-cell migration trajectories on different Ti surfaces.

Acknowledgements

Thanks for Mr. Li for your understanding and support during my work.

Author contributions

Y.Z., K.L., and G.L. contributed equally to this work. Y.Z., K.L. designed the experiments and prepared the manuscript. Y.Z., K.L., and G.L. performed most of the experiments and collected the data. Y.W. analyzed and visualized the data. Y.H., W.S. and Y.Z. sponsored the research, reviewed the manuscript and provided scientific consultation along the study.

Funding

The work is supported by National Natural Science Foundation of China (32071324, 82271029 and 82101064), Shaanxi Provincial Key Research and Development Plan Project (2023-YBSF-559).

Data Availability

The datasets used and/or analyzed during the current study are available from the corresponding author on reasonable request.

Declarations

Ethics approval and consent to participate

All experimental protocols were approved by the Animal Care Committee of the Fourth Military Medical University (FMMU), which was in accordance with the NIH Guide for the Care and Use of Laboratory Animals.

Consent for publication

All authors are consent for publication.

Competing interests

The authors declare no competing interests.

Author details

¹State Key Laboratory of Oral & Maxillofacial Reconstruction and Regeneration, National Clinical Research Center for Oral Diseases, Shaanxi Key Laboratory of Stomatology, Department of Prosthodontics, School of Stomatology, The Fourth Military Medical University, Xi'an, Shaanxi 710032, China

²Department of stomatology, The 986th Air Force Hospital, Xijing Hospital, The Fourth Military Medical University, Xi'an, Shaanxi 710032, China

³State Key Laboratory of Oral & Maxillofacial Reconstruction and Regeneration, National Clinical Research Center for Oral Diseases, Shaanxi International Joint Research Center for Oral Diseases, Department of Periodontology, School of Stomatology, The Fourth Military Medical University, Xi'an, Shaanxi 710032, China

⁴State Key Laboratory of Oral & Maxillofacial Reconstruction and Regeneration, National Clinical Research Center for Oral Diseases, Shaanxi Key Laboratory of Stomatology, Department of Operative Dentistry and Endodontics, School of Stomatology, The Fourth Military Medical University, Xi'an, Shaanxi 710032, China

Received: 27 October 2023 / Accepted: 3 December 2023

Published online: 08 December 2023

References

- Dong Z, Peng R, Zhang Y, Shan Y, Ding W, Liu Y, et al. Tendon repair and regeneration using bioinspired fibrillation engineering that mimicked the structure and mechanics of natural tissue. *ACS Nano*. 2023;17(18):17858–72.
- Wang F, Qiu T, Ling Y, Yang Y, Zhou Y. Physical and chemical cues at the nano–Bio interface for immunomodulation. *Angew Chem Int Ed*. 2022;61(41):e202209499.
- Bai L, Chen P, Zhao Y, Hang R, Yao X, Tang B, et al. A micro/nano-biomimetic coating on titanium orchestrates osteo/angio-genesis and osteoimmunomodulation for advanced osseointegration. *Biomaterials*. 2021;278:121162.
- Zhang Z, Xu R, Yang Y, Liang C, Yu X, Liu Y, et al. Micro/nano-textured hierarchical titanium topography promotes exosome biogenesis and secretion to improve osseointegration. *J Nanobiotechnol*. 2021;19(1):78.
- Kong K, Chang Y, Hu Y, Qiao H, Zhao C, Rong K, et al. TiO₂ nanotubes promote osteogenic differentiation through regulation of Yap and Piezo1. *Front Bioeng Biotechnol*. 2022;10:872088.
- He Y, Luo J, Zhang Y, Li Z, Chen F, Song W, et al. The unique regulation of implant surface nanostructure on macrophages M1 polarization. *Mater Sci Eng C*. 2020;106:110221.
- Li X, Klausen LH, Zhang W, Jahed Z, Tsai CT, Li TL, et al. Nanoscale Surface topography reduces focal adhesions and cell stiffness by enhancing integrin endocytosis. *Nano Lett*. 2021;21(19):8518–26.
- Yang Q, Miao Y, Banerjee P, Hourwitz MJ, Hu M, Qing Q, et al. Nanotopography modulates intracellular excitable systems through cytoskeleton actuation. *Proc Natl Acad Sci*. 2023;120(19):e2218906120.
- Previdi A, Borghi F, Profumo F, Schulte C, Piazzoni C, Lamanna J, et al. Nanotopography and Microconfinement Impact on primary hippocampal astrocyte morphology, Cytoskeleton and spontaneous calcium Wave Signalling. *Cells*. 2023;12(2):293.
- Lestrell E, Chen Y, Aslanoglou S, O'Brien CM, Elnathan R, Voelcker NH. Silicon Nanoneedle-Induced Nuclear deformation: implications for human somatic and stem cell nuclear mechanics. *ACS Appl Mater Interfaces*. 2022;14(40):45124–36.
- Park J, Bauer S, Schlegel KA, Neukam FW, Von Der Mark K, Schmuki P. TiO₂ Nanotube surfaces: 15 nm—An optimal length scale of Surface topography for cell adhesion and differentiation. *Small*. 2009;5(6):666–71.
- Parisi L, Ghezzi B, Bianchi MG, Toffoli A, Rossi F, Bussolati O, et al. Titanium dental implants hydrophilicity promotes preferential serum fibronectin over albumin competitive adsorption modulating early cell response. *Mater Sci Eng C*. 2020;117:111307.
- Wu C, Tang Y, Mao B, Yan X, Pu Y, Zhao K. Improved hydrophilicity and durability of polarized PVDF coatings on anodized titanium surfaces to enhance mineralization ability. *Colloids Surf B Biointerfaces*. 2021;205:111898.
- Ghezzi B, Lagonegro P, Attolini G, Rotonda PM, Cornelissen C, Ponraj JS, et al. Hydrogen plasma treatment confers enhanced bioactivity to silicon carbide-based nanowires promoting osteoblast adhesion. *Mater Sci Eng C*. 2021;121:111772.
- Rupp F, Liang L, Geis-Gerstorfer J, Scheideler L, Hüttig F. Surface characteristics of dental implants: a review. *Dent Mater*. 2018;34(1):40–57.
- Rodríguez-González R, Monsalve-Guil L, Jiménez-Guerra A, Velasco-Ortega E, Moreno-Muñoz J, Nuñez-Marquez E, et al. Relevant aspects of titanium topography for Osteoblastic adhesion and inhibition of Bacterial colonization. *Materials*. 2023;16(9):3553.
- Abuna RPF, Oliveira FS, Adolpho LF, Fernandes RR, Rosa AL, Beloti MM. Frizzled 6 disruption suppresses osteoblast differentiation induced by nanotopography through the canonical wnt signaling pathway. *J Cell Physiol*. 2020;235(11):8293–303.
- Cimpean A, Neacsu P, Mazare A, Schmuki P. Attenuation of the macrophage inflammatory activity by TiO₂ nanotubes via inhibition of MAPK and NF- κ B pathways. *Int J Nanomedicine*. 2015; 10:6455–67.

19. Wang W, Liu Q, Zhang Y, Zhao L. Involvement of ILK/ERK1/2 and ILK/p38 pathways in mediating the enhanced osteoblast differentiation by micro/nanotopography. *Acta Biomater*. 2014;10(8):3705–15.
20. Wang W, Li G, Wang J, Song W, Luo J, Meng F, et al. Involvement of Rac1 in the micro/nano-topography sensing and osteogenic differentiation in bone marrow mesenchymal stem cells. *Mater Des*. 2018;157:402–11.
21. Liu Q, Wang W, Zhang L, Zhao L, Song W, Duan X, et al. Involvement of N-cadherin/ β -catenin interaction in the micro/nanotopography induced indirect mechanotransduction. *Biomaterials*. 2014;35(24):6206–18.
22. Patergnani S, Danese A, Bouhamida E, Aguiari G, Previati M, Pinton P, et al. Various aspects of Calcium Signaling in the regulation of apoptosis, Autophagy, Cell Proliferation, and Cancer. *Int J Mol Sci*. 2020;21(21):8323.
23. Li G, Chang B, He Y, Li Y, Liu J, Zhang Y, et al. Orai1 mediated store-operated calcium entry contributing to MC3T3-E1 differentiation on titanium implant with micro/nano-textured topography. *Biomater Adv*. 2022;133:112644.
24. Cui C, Merritt R, Fu L, Pan Z. Targeting calcium signaling in cancer therapy. *Acta Pharm Sin B*. 2017;7(1):3–17.
25. Hammad AS, Machaca K. Store Operated Calcium Entry in Cell Migration and Cancer Metastasis. *Cells*. 2021;10(5):1246.
26. Lin YS, Lin YH, Nguyen Thi M, Hsiao SC, Chiu WT. STIM1 controls the Focal Adhesion Dynamics and Cell Migration by regulating SOCE in Osteosarcoma. *Int J Mol Sci*. 2021;23(1):162.
27. Wang W, Zhao L, Wu K, Ma Q, Mei S, Chu PK, et al. The role of integrin-linked kinase/ β -catenin pathway in the enhanced MG63 differentiation by micro/nano-textured topography. *Biomaterials*. 2013;34(3):631–40.
28. Youvan DC, Silva CM, Bylina EJ, Coleman WJ, Dilworth MR, Yang MM. Calibration of fluorescence resonance energy transfer in microscopy using genetically engineered GFP derivatives on nickel chelating beads. *Biotechnology*. 1997. DOI:US6456734B1.
29. Bootman MD. Calcium Signaling. *Cold Spring Harb Perspect Biol*. 2012;4(7):a011171.
30. Oh S, Brammer KS, Li YSJ, Teng D, Engler AJ, Chien S, et al. Stem cell fate dictated solely by altered nanotube dimension. *Proc Natl Acad Sci*. 2009;106(7):2130–5.
31. Charras GT, Williams BA, Sims SM, Horton MA. Estimating the sensitivity of Mechanosensitive Ion Channels to membrane strain and tension. *Biophys J*. 2004;87(4):2870–84.
32. Blumenthal NR, Hermanson O, Heimrich B, Shastri VP. Stochastic nanoroughness modulates neuron–astrocyte interactions and function via mechanosensing cation channels. *Proc Natl Acad Sci*. 2014;111(45):16124–9.
33. Fujii S, Ushioda R, Nagata K. Redox states in the endoplasmic reticulum directly regulate the activity of calcium channel, inositol 1,4,5-trisphosphate receptors. *Proc Natl Acad Sci*. 2023;120(22):e2216857120.
34. Prakriya M, Lewis RS. STORE-OPERATED CALCIUM CHANNELS. *Physiol Rev*. 2015;95(4):1383–436.
35. Vaeth M, Kahlfuss S, Feske S. CRAC Channels and Calcium Signaling in T cell-mediated immunity. *Trends Immunol*. 2020;41(10):878–901.
36. Gross SA, Wissenbach U, Philipp SE, Freichel M, Cavalieri A, Flockerzi V. Murine ORAI2 splice variants Form Functional Ca²⁺ + release-activated Ca²⁺ (CRAC) channels. *J Biol Chem*. 2007;282(27):19375–84.
37. Brandman O, Liou J, Park WS, Meyer T. STIM2 is a Feedback Regulator that stabilizes basal cytosolic and endoplasmic reticulum Ca²⁺ + levels. *Cell*. 2007;131(7):1327–39.
38. Luo Y, Ye J, Deng Y, Huang Y, Liu X, He Q, et al. The miRNA-185-5p/STIM1 Axis regulates the invasiveness of Nasopharyngeal Carcinoma Cell Lines by modulating EGFR activation-stimulated switch from E- to N-Cadherin. *Molecules*. 2023;28(2):818.
39. Parekh AB. Store-operated CRAC channels: function in health and Disease. *Nat Rev Drug Discov*. 2010;9(5):399–410.
40. Mengqi S, Wen S, Boxin Z, Minni L, Yan Z, Qun W, et al. Micro/nano topography with altered nanotube diameter differentially trigger endoplasmic reticulum stress to mediate bone mesenchymal stem cell osteogenic differentiation. *Biomed Mater*. 2021;16(1):015024.
41. Kania E, Pająk B, Orzechowski A. Calcium Homeostasis and ER Stress in Control of Autophagy in Cancer Cells. *BioMed Res Int*. 2015; 2015:352794.
42. Algar WR, Hildebrandt N, Vogel SS, Medintz IL. FRET as a biomolecular research tool — understanding its potential while avoiding pitfalls. *Nat Methods*. 2019;16(9):815–29.
43. Emrich SM, Yoast RE, Trebak M. Physiological functions of CRAC channels. *Annu Rev Physiol*. 2022;84(1):355–79.
44. He J, Liu Q, Zheng S, Shen R, Wang X, Gao J, et al. Enlargement, reduction, and even reversal of relative Migration speeds of endothelial and smooth muscle cells on Biomaterials simply by adjusting RGD Nanospacing. *ACS Appl Mater Interfaces*. 2021;13(36):42344–56.
45. Liu Q, Zheng S, Ye K, He J, Shen Y, Cui S, et al. Cell migration regulated by RGD nanospacing and enhanced under moderate cell adhesion on biomaterials. *Biomaterials*. 2020;263:120327.
46. Slater JH, Boyce PJ, Jancaitis MP, Gaubert HE, Chang AL, Markey MK, et al. Modulation of endothelial cell migration via manipulation of adhesion site growth using nanopatterned surfaces. *ACS Appl Mater Interfaces*. 2015;7(7):4390–400.
47. Nagano M, Hoshino D, Koshikawa N, Akizawa T, Seiki M. Turnover of focal adhesions and Cancer Cell migration. *Int J Cell Biol*. 2012;2012:310616.
48. D'Souza RS, Lim JY, Turgut A, Servage K, Zhang J, Orth K, et al. Calcium-stimulated disassembly of focal adhesions mediated by an ORP3/IQSec1 complex. *eLife*. 2020;9:e54113.
49. Cavalcanti-Adam EA, Volberg T, Micoulet A, Kessler H, Geiger B, Spatz JP. Cell spreading and focal Adhesion dynamics are regulated by spacing of integrin ligands. *Biophys J*. 2007;92(8):2964–74.
50. Levario-Diaz V, Alvarado RE, Rodriguez-Quinteros CM, Fink A, Christian J, Feng W, et al. 1D micro-nanopatterned integrin ligand surfaces for directed cell movement. *Front Cell Dev Biol*. 2022;10:972624.
51. Zhang X, Tee YH, Heng JK, Zhu Y, Hu X, Margadant F, et al. Kinectin-mediated endoplasmic reticulum dynamics supports focal adhesion growth in the cellular lamella. *J Cell Sci*. 2010;123(Pt 22):3901–12.
52. Guadagno NA, Margiotta A, Bjørnstad SA, Haugen LH, Kjos I, Xu X, et al. Rab18 regulates focal adhesion dynamics by interacting with kinectin-1 at the endoplasmic reticulum. *J Cell Biol*. 2020;219(7):e201809020.
53. Silver K, Littlejohn A, Thomas L, Bawa B, Lillich JD. Suppression of calpain expression by NSAIDs is associated with inhibition of cell migration in rat duodenum. *Toxicology*. 2017;383:1–12.
54. Frith JE, Mills RJ, Cooper-White JJ. Lateral spacing of adhesion peptides influences human mesenchymal stem cell behaviour. *J Cell Sci*. 2012;125(2):317–27.

Publisher's Note

Springer Nature remains neutral with regard to jurisdictional claims in published maps and institutional affiliations.